Floquet-driven crossover from density-assisted tunneling to enhanced pair tunneling

Nick Klemmer,[1, *] Janek Fleper,[1, *] Valentin Jonas,[1] Ameneh Sheikhan,[1]
Corinna Kollath,[1] Michael Köhl,[1] and Andrea Bergschneider[1]

[1]*Physikalisches Institut, University of Bonn, 53115 Bonn, Germany*

We investigate the experimental control of pair tunneling in a double-well potential using Floquet engineering. We demonstrate a crossover from a regime with density-assisted tunneling to dominant pair tunneling by tuning the effective interactions. Furthermore, we show that the pair tunneling rate can be enhanced not only compared to the Floquet-reduced single-particle tunneling but even beyond the static superexchange rate, while keeping the effective interaction in a relevant range. This opens possibilities to realize models with explicit pair tunneling in ultracold atomic systems.

Understanding the complexity of correlated quantum matter from microscopic principles is a notoriously difficult challenge. One example of a bottom-up approach is the Hubbard model, which strives to explain macroscopic quantum states by the two elementary processes: single-particle tunneling t between neighboring lattice sites and two-particle on-site interaction of strength U, see Figure 1(a). Within this framework, one is able to explain the occurrence of Mott insulators [1, 2], superconductors [3] or quantum magnets [4–6], and their fundamental properties. However, the Hubbard model makes substantial simplifications in the description of matter: tunneling processes, for example, are always that of single particles and neither tunneling of pairs nor density-assisted tunneling, where the tunneling depends on the occupation of the site, are explicitly accounted for. Instead, pair tunneling only arises implicitly as a second-order process at strong interactions ($|U| > t$). There, the interaction favors correlated tunneling of single particles through a virtual state with a rate proportional to $\sim t^2/|U|$, see Figure 1(c)-(e). This superexchange process as well as density-assisted tunneling have been observed with ultracold atoms in double-well potentials [7, 8] and optical lattices [9, 10].

It has been theoretically predicted that explicit pair tunneling as well as density-assisted tunneling of a significant strength give rise to novel quantum phases [11–15] beyond the standard Hubbard model. An effective, density-assisted tunneling process is required for mapping a three-orbital model to a single-orbital model [16], and explicit pair tunneling as realized in the Penson-Kolb-Hubbard model [17], can induce, for instance, η-pairing phases [11, 12]. Moreover, in the absence of single-particle tunneling an explicit pair tunneling has been predicted to lead to topologically non-trivial phases by the induced symmetries [13–15]. Such phases are yet elusive in static realizations since pair tunneling is usually suppressed significantly as compared to single-particle tunneling by the larger mass of the pairs.

In recent years, Floquet engineering [18–20] has been developed to control parameters and quantum phases in ultracold atom systems [21–25]. The key idea of Floquet engineering is to periodically drive a system parameter, such as the potential bias between neighbouring lattice sites, at a high frequency. In an effective, time-independent description this leads to a renormalized tunneling t_{eff} and interaction strength U_{eff}, see Figure 1(b). Using Floquet engineering, researchers have demonstrated to suppress single-particle tunneling [21], induce density-assisted tunneling [22, 26], or invert the sign of magnetic correlations [26], to name just a few examples, and it seems worthwhile to explore its potential benefits with regards to the control of pair tunneling, too. However, the Floquet engineering comes at a cost: for a resonant Floquet drive the effective interaction energy is nulled [27].

In this work, we demonstrate experimentally a crossover from a density-assisted tunneling to an enhanced pair-tunneling regime via Floquet engineering by tuning the driving frequency with respect to the static on-site interaction. First, we study density-assisted tunneling in effectively non-interacting driven double wells while fully suppressing single-particle tunneling. Then, we introduce effective interactions and demonstrate the enhancement of pair tunneling by suppressing the population of the intermediate state in which the populations are split between the sites (cf. Figure 1(c)). An especially intriguing finding is that for large effective interactions the pair tunneling rate can be enhanced significantly above the superexchange rate of the corresponding time-independent effective description of the double well.

We perform our experiment using a quantum degenerate sample of ^{40}K atoms in the lowest two hyperfine states, denoted as $|\uparrow\rangle$ and $|\downarrow\rangle$. The atoms are confined in a three-dimensional optical lattice formed by off-resonant laser beams. Along the x-direction, the optical lattice is bichromatic and composed of two retro-reflected laser beams of an infrared (1064 nm) and a green (532 nm) wavelength in order to form a chain of tunable double wells. We achieve tunability of the barrier heights within and between the double wells as well as of the potential bias between the sites of each double well by controlling both laser powers and frequencies [7, 28]. In all experiments discussed here, we focus on isolated double wells by suppressing the tunneling amplitude between double wells using a depth of $15\,E_{\text{rec}}$ ($12\,E_{\text{rec}}$) for the 1064 nm (532 nm) lattice while freezing the dynamics along y- and z-directions with lattice depths of $60\,E_{\text{rec}}$ and $110\,E_{\text{rec}}$, respectively. Here, $E_{\text{rec}} = h/(2m\lambda^2)$ denotes the recoil

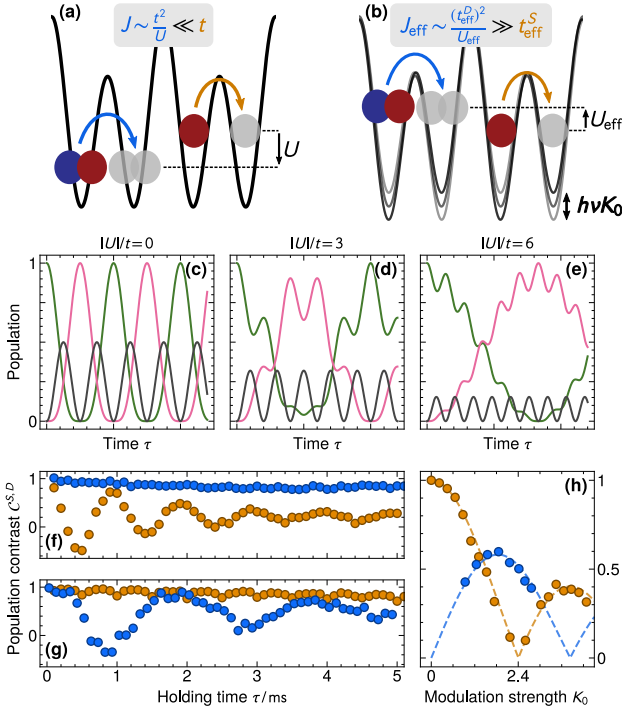arXiv:2404.08482v1 [cond-mat.quant-gas] 12 Apr 2024

FIG. 1. Controlling tunneling dynamics in static and driven double wells. (a) In the static double well, single-particle tunneling t and the on-site interaction U lead to the two-particle tunneling $J \ll t$. (b) In a driven double well with driving frequency ν and amplitude $h\nu K_0$, the effective pair-tunneling rate can exceed the effective single-particle tunneling rates $J_{\text{eff}} \gg t^S_{\text{eff}}$. (c)-(e) Tunneling dynamics with negligible to strong interaction. In a non-interacting system at half filling (c), the pair tunnels from the left lattice site (green) to the right lattice site (pink) by going through the split state (black). For larger interactions (d,e), the population of the split state is significantly suppressed. Measured tunneling dynamics at $U/t \approx -9$ for the static (f) and resonantly driven double well (g) with driving frequency $\nu = |U|/h$ and amplitude $K_0 = 2.4$. The population contrast between left and right lattice sites is measured for quarter-filled $\mathcal{C}^S$ (orange) and half-filled double wells $\mathcal{C}^D$ (blue). (h) Effective tunnel coupling of resonantly driven double wells extracted from tunneling dynamics. In quarter-filled (half-filled) double wells, the tunneling follows a 0th-order Bessel function $\mathcal{J}_0(K_0)$ (1st-order Bessel function $\mathcal{J}_1(K_0)$) in orange (blue), respectively.

energy for atoms with mass m in an optical lattice of wavelength λ and h is Planck's constant. In this work, we choose $t/h = 480\,\text{Hz}$ and an interaction strength of $U/t \approx -9$, if not stated otherwise.

We begin our experimental sequence by loading a balanced spin mixture into the lowest Bloch band of the infrared lattice along the x–direction. This results in an occupation of at most one $|\uparrow\rangle$ and one $|\downarrow\rangle$ atom per lattice site. Subsequently, the green lattice is adiabatically ramped up to $25\,E_{\text{rec}}$ at a significant potential bias $|\Delta_0| \gg t, |U|$ between the left and right site of the resulting double-well array to ensure population of only the

left sublattice site. This produces either half-filled double wells (a pair with one $|\uparrow\rangle$ and one $|\downarrow\rangle$ atom), quarter-filled double wells (with either a $|\uparrow\rangle$ or a $|\downarrow\rangle$ atom) or empty double wells in rare cases. In the first experiment, we then induce tunneling oscillations between left and right sites by removing the potential bias and simultaneously unfreezing the lattice within $100\,\mu\text{s}$ in a diabatic fashion. During the following time evolution, the system can be described by an array of double-well Hamiltonians

$$\hat{H} = -t \sum_\sigma \left(\hat{c}^\dagger_{L\sigma} \hat{c}_{R\sigma} + h.c. \right)$$
$$+ U \sum_i \hat{n}_{i\uparrow} \hat{n}_{i\downarrow} + \sum_\sigma \frac{\Delta_0}{2} (\hat{n}_{L\sigma} - \hat{n}_{R\sigma}),$$

with the fermionic raising (lowering) operators $\hat{c}_{i\sigma}$ ($\hat{c}^\dagger_{i\sigma}$), and the number operator $\hat{n}_{i\sigma} = \hat{c}^\dagger_{i\sigma} \hat{c}_{i\sigma}$ at sublattice site $i = L, R$ in spin state $\sigma = \uparrow, \downarrow$. After a holding time τ, we freeze the dynamics and detect the system by resolving single and double occupancies at left and right sites of the double wells. To resolve the site occupation, we transfer atoms at left (right) sites to the first (third and fourth) Bloch band of the superlattice and then employ an adiabatic band-mapping technique [7, 28, 29]. From the measured Brillouin-zone occupations N_1 and $N_{34} = N_3 + N_4$, we extract the site occupation-resolved population contrast $\mathcal{C}^S$ ($\mathcal{C}^D$) between left and right lattice sites with single occupancy (double occupancy), where $\mathcal{C} = (N_1 - N_{34}) / (N_1 + N_{34})$.

The tunneling dynamics in the static double well with strong attractive interaction is shown in Figure 1(f). While for quarter-filled double wells, the atoms tunnel between the lattice sites, an almost constant population contrast is measured for the half-filled double wells due to the small pair-tunneling rates. The observed dephasing of the oscillation mainly stems from the Gaussian envelope of our lattice laser beams, resulting in approximately $20\,\%$ variation in the tunneling strength t and $10\,\%$ in the interaction strength U, as well as a small, position-dependent bias Δ_0 between adjacent lattice wells.

A periodic modulation of the system can fundamentally alter the tunneling dynamics [21, 24, 25, 30]. In particular, a high-frequency drive close to resonance with the interaction energy $\ell\nu \approx |U|/h \gg t/h$, where ℓ is an integer and denotes the harmonic order, alters the dynamics in quarter- and half-filled double wells in different ways. For the half-filled double wells, the near-resonant drive modifies the interaction energy $U_{\text{eff}} = U + \ell h\nu$, for $U < 0$, and introduces density-assisted tunneling with amplitude $t^{(\ell)}_{\text{eff}} = t\mathcal{J}_\ell(K_0)$ [22, 27, 32]. At the same time, in quarter-filled double wells, the modulation frequency is the highest energy scale and reduces the single-particle tunneling amplitude to $t^S_{\text{eff}} = t\mathcal{J}_0(K_0)$ [30, 31]. We will show that this interplay of effective interactions and density-assisted tunneling can introduce significant pair tunneling $\hat{c}^\dagger_{R\uparrow} \hat{c}^\dagger_{R\downarrow} \hat{c}_{L\uparrow} \hat{c}_{L\downarrow}$ with amplitude J_{eff} independent of t^S_{eff}.

We realize the periodically modulated system by starting with the preparation as in the static case discussed be-

fore where particles are localized at the left sublattice sites. Then, we adiabatically ramp on a periodic modulation of the double-well bias $\Delta_0 \to \Delta(\tau) = \Delta_0 + h\nu K_0 \cos(2\pi\nu\tau)$ at a frequency ν and amplitude $h\nu K_0$. Subsequently, we unfreeze and measure the tunneling dynamics of the Floquet-driven double well [33–36] by extracting $\mathcal{C}^{S,D}(\tau)$. The resulting dynamics for a resonant drive $\nu = |U|/h \gg t$ and $K_0 = 2.4$ is shown in Figure 1 (g). In contrast to the static case, the quarter-filled double wells dynamically localize while for the half-filled double wells, the resonant drive balances the interaction energy and introduces density-assisted tunneling with about half the frequency as for the static system. In Figure 1(h), we show the different effective tunneling amplitudes of quarter- and half-filled double wells for different driving strength following the Bessel functions of different orders. This shows that the periodic drive can be employed in order to tune the ratio of the single-particle to density-assisted tunneling over a wide range.

In the following, we study the crossover from density-assisted tunneling to pair-tunneling by introducing effective interactions. To this end, we detune the driving frequency from resonance while suppressing the single-particle tunneling via the driving amplitude $K_0 = 2.4$. The impact of effective interactions and higher order tunneling processes on the dynamic signals is shown in Figure 2. For an effectively non-interacting system with $\nu \approx |U|/h$ (see Figure 2(a)) the oscillation dynamics exhibit a single characteristic frequency. Upon introducing a small detuning of the driving frequency from the resonance, a beating becomes apparent in the contrast measurement (see Figure 2(b)-(e)). This beating becomes more pronounced with increasing detuning and is accompanied by a decrease in oscillation amplitude. When the driving frequency is approximately $\nu \approx U/(2h)$ (cf. Figure 2(e)), the oscillation amplitude increases again and the characteristic signature of frequency beating is less pronounced. This indicates that another effectively non-interacting system is realized by the second-harmonic resonance condition [23, 24].

We compare our experimental data to theoretical calculations using Floquet theory to determine the time-independent effective Floquet Hamiltonian for a near-resonant drive [18, 19, 37]. For this purpose, we employ a high-frequency expansion of the Floquet Hamiltonian up to the third order in $1/\nu$, while incorporating the Bessel functions $\mathcal{J}_j(K_0)$ for $j = 0, 1, 2, 3$ [37, 38]. In order to account for the inhomogeneous intensity distribution of our optical lattice in our theoretical analysis, we calculate the spatially dependent Floquet and Hubbard parameters $K_0(\boldsymbol{x})$, $t(\boldsymbol{x})$, $U(\boldsymbol{x})$, and $\Delta_0(\boldsymbol{x})$. To obtain t, we compute the Wannier functions using the band-projected position operator method [39, 40] and use this to calculate U based on the s–wave scattering length a [41, 42]. With these parameters, we solve the different Floquet-driven double-well Hamiltonians and compute the time- and position-dependent contrast $\mathcal{C}^D(\boldsymbol{x}, \tau)$. We then perform a density-weighted average over the inhomogeneous den-
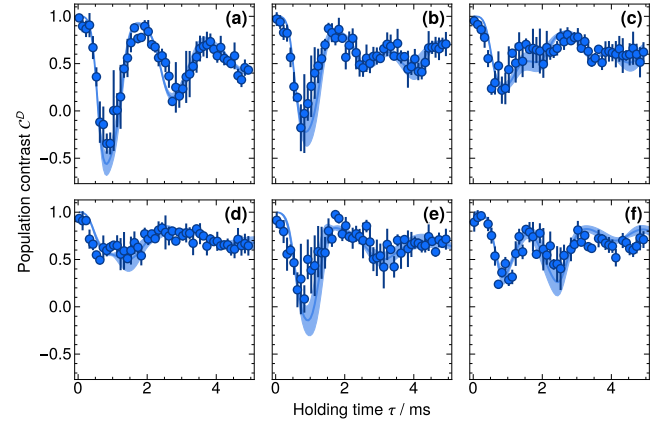

FIG. 2. Measured dynamics in driven, half-filled double wells and attractive interaction $U/h \approx -4\,\mathrm{kHz}$ ($U/t \approx -9$). The measured population contrast $\mathcal{C}^{\mathcal{D}}$ is shown for driving amplitude $K_0 = 2.4$ and driving frequencies: 4.05 kHz, 3.9 kHz, 3.6 kHz, 2.7 kHz, 2.25 kHz and 2.05 kHz (a to f). The fitted time evolution of the global Hamiltonian is shown as solid blue line and the shaded regions indicate the 1σ confidence intervals.

sity distribution resulting in the global observable $\mathcal{C}^D(\tau)$. To account for experimental fluctuations, this contrast is then fitted to our experimental data leaving the scattering length a and the green lattice potential depth at the trap center as fit parameters. The fitted results are presented as solid lines in Figure 2, with the 1σ confidence interval due to residual uncertainties of the Floquet and Hubbard parameters indicated by a shaded region. The numerical data accurately replicates the dynamic features observed in our experimental data as well as a pronounced dephasing. The fitted scattering lengths and lattice depths are in good agreement with our experimental uncertainties.

To gain valuable insight on the effective processes that cause the observed dynamics, we extract the energy spectrum of the fitted effective Hamiltonian at the trap center for half-filling. This procedure provides three relevant energy eigenvalues per driving frequency, shown in Figure 3(a), and a fourth eigenvalue, which is constant zero due to a lack of coupling and hence omitted from display. The rescaled energy spectrum $E/h\nu$ as a function of the normalized driving frequency $h\nu/|U|$ reveals two distinct avoided crossings at $\nu \approx |U|/h$ and $\nu \approx |U|/(2h)$ corresponding to the two lowest harmonics. At the avoided crossings the system is effectively non-interacting and the energy gap between the eigenstates corresponds to the induced density-assisted tunneling $2\,t_{\mathrm{eff}}^{(\ell)}$. Above resonance, the emerging effective repulsive interaction strength $U_{\mathrm{eff}} \approx U + \ell h\nu > 0$ pushes the upper two energy branches up in an approximately linear fashion due to their increasing contribution of double occupancies. Similarly, below resonance, the energy of the lower two branches is decreased by the attractive interaction.

We further analyze the effective processes by extracting the minimal energy difference $\Delta E_{\mathrm{min}}/(2t)$ between two
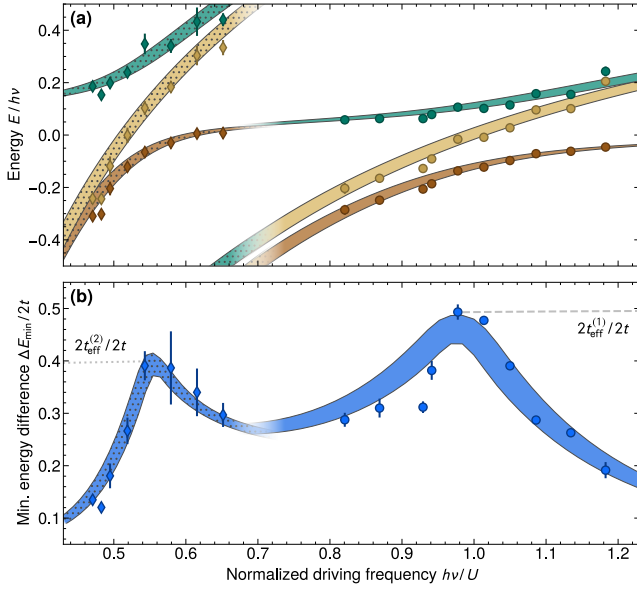
FIG. 3. Spectrum of the effective Hamiltonian for half-filled double wells. (a) Extracted energy eigenvalues $E/(h\nu)$ of the fitted Hamiltonian at the trap center for various driving frequencies $h\nu/U$ at a driving amplitude $K_0 = 2.4$ for the first (second) harmonic near-resonant case as circles (diamonds). (b) Minimal energy difference $\Delta E_{\min}/(2t)$ between two energy eigenstates of the spectrum. The effective single-particle tunneling amplitudes for the effectively non-interacting systems t_{eff}^{ℓ} are indicated as dashed lines. The 1σ confidence interval of the first (second) harmonic near-resonant theory is shown as a shaded (hatched) region applying to both subplots.

eigenstates in the spectrum (see Figure 3(b)). For effectively non-interacting systems at resonance, this quantity corresponds to the density-assisted tunneling amplitude $2t_{\mathrm{eff}}^{(\ell)}$ that follows to lowest order the Bessel functions $\mathcal{J}_\ell(K_0)$ depending on the harmonic order ℓ as indicated by the gray dashed lines. Far from resonance, the arising large effective interactions suppress the breaking of the pairs and the minimal energy gap corresponds to the effective pair tunneling $|J_{\mathrm{eff}}|$. Note, that for the chosen parameters both tunneling processes are larger than the effective single-particle tunneling, which enables the realization of models with dominant higher-order tunneling processes.

To map out the crossover from density-assisted tunneling to the pair tunneling, we quantify the pair splitting by the time-averaged population of split pairs $A_{\mathrm{split}} = \overline{|\langle LR|\Psi(\tau)\rangle|^2 + |\langle RL|\Psi(\tau)\rangle|^2}$. From this, we extract the pair-tunneling fidelity $\mathcal{F}_{\mathrm{pair}} = 1 - 4A_{\mathrm{split}}$ of the driven system (see Figure 4(a)). As expected, pair tunneling becomes more pronounced for larger effective interaction strength. For ($|U_{\mathrm{eff}}/t_{\mathrm{eff}}| > 5$), this fidelity exceeds $60\,\%$, rendering pair tunneling the dominant process in the time evolution of the system. Surprisingly, the pair-tunneling rate in the driven system is also enhanced significantly compared to its static counterpart. We show this in
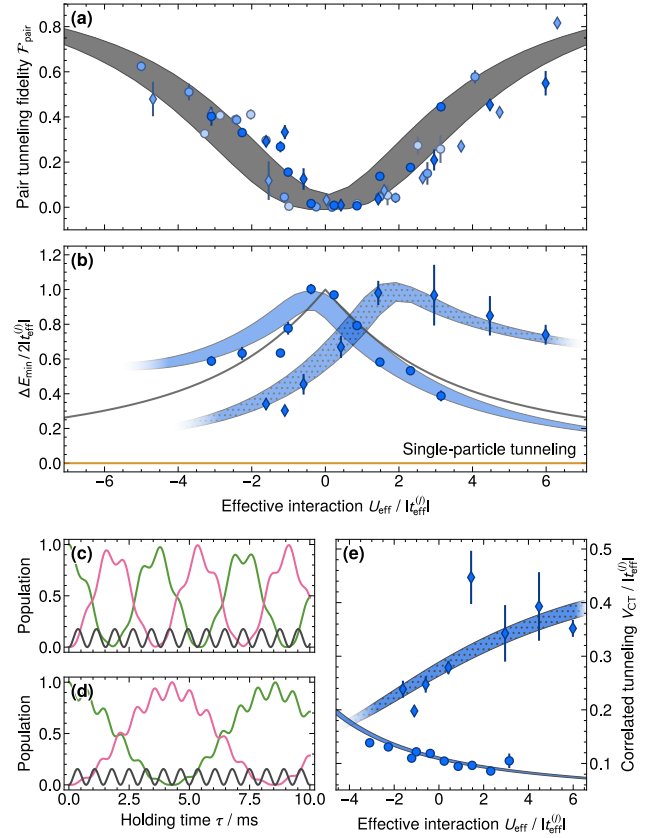

FIG. 4. (a) The pair-tunneling fidelity $\mathcal{F}_{\mathrm{pair}}$ is determined as a function of the effective interaction strength $U_{\mathrm{eff}}/|t_{\mathrm{eff}}^{(\ell)}|$ for various absolute interaction strengths $U/t \approx -9$ (dark blue), $U/t \approx -18$ (blue) and $U/t \approx -6$ (light blue) as circles (diamonds) for the first (second) harmonic resonance. (b) The minimal energy difference $\Delta E_{\min}/(2|t_{\mathrm{eff}}^{(\ell)}|)$ is shown as a function of the effective interaction strength $U_{\mathrm{eff}}/|t_{\mathrm{eff}}^{(\ell)}|$ for $U/t = -9$ and compared to the static double well (solid grey line) and the single-particle tunneling (orange line). (c) In the driven double well with harmonic order $\ell = 2$ and effective interaction strength $U_{\mathrm{eff}}/|t_{\mathrm{eff}}^{(2)}| = 6$ the pair tunnels from the left lattice site (green) to the right lattice site (pink) with only a reduced population of the split states (black) and higher frequency compared to the static double well (d). (e) The extracted correlated tunneling rate $V_{\mathrm{CT}}/|t_{\mathrm{eff}}^{(\ell)}|$ is given as a function of the effective interaction strength $U_{\mathrm{eff}}/t_{\mathrm{eff}}^{(\ell)}$ for $U/t = -9$. For all subplots, the 1σ confidence interval of the first (second) harmonic near-resonant theory is shown as a shaded (hatched) region.

Figure 4(b), where we compute the minimal energy gap rescaled by the effective density-assisted tunneling at the associated resonance $\Delta E_{\min}/(2|t_{\mathrm{eff}}^{(\ell)}|)$ versus the normalized effective interaction strength $U_{\mathrm{eff}}/|t_{\mathrm{eff}}^{(\ell)}|$. We compare this to the minimal energy gap of a static system (solid gray line) which corresponds to the single-particle tunneling for a non-interacting system and approaches the superexchange rate $4t^2/U$ for large interactions. Interestingly, for large effective interactions this minimal energy

difference can be enhanced compared to the static counterpart (see grey line in Fig. 4(b)). In particular, at an effective repulsive interaction of $U_{\text{eff}}/|t_{\text{eff}}| \approx 6$, this enhancement reaches more than a factor of two for the second-harmonic resonance. The main reason for this is the appearance of an explicit correlated tunneling amplitude V_{CT} in the effective Hamiltonian, that enhances the pair-tunneling amplitude $J_{\text{eff}} = (-1)^{\ell} 4(t_{\text{eff}}^{(\ell)})^2/U_{\text{eff}} + V_{\text{CT}}$ above the superexchange rate of the static counterpart (cf. Figure 4(c) and (d)). Note that the harmonic order ℓ changes the sign of the superexchange contribution [26], leading to the asymmetry between the two harmonic resonances in Fig. 4(b). Moreover, the frequency dependence of the correlated tunneling $V_{\text{CT}} \sim t^2/h\nu$, shown in Figure 4(e), causes the observed deviation from the static counterpart, which is more pronounced for the second-harmonic resonance than for the first-harmonic.

In conclusion, we have utilized Floquet engineering to realize a crossover from density-assisted tunneling to pair tunneling in an effectively interacting system, while simultaneously suppressing single-particle tunneling. We could further demonstrate that the realized pair tunneling rate is significantly enhanced beyond the expectations from superexchange processes in their static equivalent. This allows for the realization of models with dominating higher-order tunneling processes [17] together with suppressed or negligible single-particle tunneling, which is not possible in the static Hubbard model.

[1] D. Greif, M. F. Parsons, A. Mazurenko, C. S. Chiu, S. Blatt, F. Huber, G. Ji, and M. Greiner, Science **351**, 953 (2016).

[2] L. W. Cheuk, M. A. Nichols, K. R. Lawrence, M. Okan, H. Zhang, and M. W. Zwierlein, Phys. Rev. Lett. **116**, 235301 (2016).

[3] D. J. Scalapino, E. Loh, and J. E. Hirsch, Phys. Rev. B **34**, 8190 (1986).

[4] M. Boll, T. A. Hilker, G. Salomon, A. Omran, J. Nespolo, L. Pollet, I. Bloch, and C. Gross, Science **353**, 1257 (2016).

[5] A. Mazurenko, C. S. Chiu, G. Ji, M. F. Parsons, M. Kanász-Nagy, R. Schmidt, F. Grusdt, E. Demler, D. Greif, and M. Greiner, Nature **545**, 462 (2017).

[6] A. Bohrdt, L. Homeier, C. Reinmoser, E. Demler, and F. Grusdt, Annals of Physics **435**, 168651 (2021), special issue on Philip W. Anderson.

[7] S. Fölling, S. Trotzky, P. Cheinet, M. Feld, R. Saers, A. Widera, T. Müller, and I. Bloch, Nature **448**, 1029 (2007).

[8] S. Trotzky, P. Cheinet, S. Fölling, M. Feld, U. Schnorrberger, A. M. Rey, A. Polkovnikov, E. A. Demler, M. D. Lukin, and I. Bloch, Science **319**, 295 (2008).

[9] F. Meinert, M. J. Mark, E. Kirilov, K. Lauber, P. Weinmann, M. Gröbner, A. J. Daley, and H.-C. Nägerl, Science **344**, 1259 (2014).

[10] O. Jürgensen, F. Meinert, M. J. Mark, H.-C. Nägerl, and D.-S. Lühmann, Phys. Rev. Lett. **113**, 193003 (2014).

[11] S. Robaszkiewicz and B. R. Bułka, Phys. Rev. B **59**, 6430 (1999).

[12] G. I. Japaridze, A. P. Kampf, M. Sekania, P. Kakashvili, and P. Brune, Phys. Rev. B **65**, 014518 (2001).

[13] C. V. Kraus, M. Dalmonte, M. A. Baranov, A. M. Läuchli, and P. Zoller, Phys. Rev. Lett. **111**, 173004 (2013).

[14] N. Lang and H. P. Büchler, Phys. Rev. B **92**, 041118 (2015).

[15] F. T. Lisandrini and C. Kollath, Phys. Rev. B **106**, 245121 (2022).

[16] S. Jiang, D. J. Scalapino, and S. R. White, Phys. Rev. B **108**, L161111 (2023).

[17] K. A. Penson and M. Kolb, Phys. Rev. B **33**, 1663 (1986).

[18] N. Goldman and J. Dalibard, Phys. Rev. X **4**, 031027 (2014).

[19] L. D. Marin Bukov and A. Polkovnikov, Advances in Physics **64**, 139 (2015).

[20] A. Eckardt, Rev. Mod. Phys. **89**, 011004 (2017).

[21] H. Lignier, C. Sias, D. Ciampini, Y. Singh, A. Zenesini, O. Morsch, and E. Arimondo, Phys. Rev. Lett. **99**, 220403 (2007).

[22] F. Meinert, M. J. Mark, K. Lauber, A. J. Daley, and H.-C. Nägerl, Phys. Rev. Lett. **116**, 205301 (2016).

[23] F. Görg, K. Sandholzer, J. Minguzzi, R. Desbuquois, M. Messer, and T. Esslinger, Nature Physics **15**, 1161 (2019).

[24] C. Schweizer, F. Grusdt, M. Berngruber, L. Barbiero, E. Demler, N. Goldman, I. Bloch, and M. Aidelsburger, Nature Physics **15**, 1168 (2019).

[25] C. Weitenberg and J. Simonet, Nature Physics **17**, 1342 (2021).

[26] F. Görg, M. Messer, K. Sandholzer, G. Jotzu, R. Desbuquois, and T. Esslinger, Nature **553**, 481 (2018).

[27] M. Messer, K. Sandholzer, F. Görg, J. Minguzzi, R. Desbuquois, and T. Esslinger, Phys. Rev. Lett. **121**, 233603 (2018).

[28] D. Pertot, A. Sheikhan, E. Cocchi, L. A. Miller, J. E. Bohn, M. Koschorreck, M. Köhl, and C. Kollath, Phys. Rev. Lett. **113**, 170403 (2014).

[29] J. Sebby-Strabley, B. L. Brown, M. Anderlini, P. J. Lee, W. D. Phillips, J. V. Porto, and P. R. Johnson, Phys. Rev. Lett. **98**, 200405 (2007).

[30] A. Eckardt, M. Holthaus, H. Lignier, A. Zenesini, D. Ciampini, O. Morsch, and E. Arimondo, Phys. Rev. A **79**, 013611 (2009).

[31] B. J. Keay, S. Zeuner, S. J. Allen, K. D. Maranowski, A. C. Gossard, U. Bhattacharya, and M. J. W. Rodwell, Phys. Rev. Lett. **75**, 4102 (1995).

[32] M. D. Liberto, C. E. Creffield, G. I. Japaridze, and C. M. Smith, Phys. Rev. A **89**, 013624 (2014).

[33] M. Grifoni and P. Hänggi, Physics Reports **304**, 229 (1998).

[34] E. Kierig, U. Schnorrberger, A. Schietinger, J. Tomkovic, and M. K. Oberthaler, Phys. Rev. Lett. **100**, 190405 (2008).

[35] Y.-A. Chen, S. Nascimbène, M. Aidelsburger, M. Atala, S. Trotzky, and I. Bloch, Phys. Rev. Lett. **107**, 210405 (2011).

[36] N. Goldman, J. Dalibard, M. Aidelsburger, and N. R. Cooper, Phys. Rev. A **91**, 033632 (2015).

[37] T. Mikami, S. Kitamura, K. Yasuda, N. Tsuji, T. Oka, and H. Aoki, Phys. Rev. B **93**, 144307 (2016).

[38] R. Desbuquois, M. Messer, F. Görg, K. Sandholzer, G. Jotzu, and T. Esslinger, Phys. Rev. A **96**, 053602 (2017).

[39] S. Kivelson, Phys. Rev. B **26**, 4269 (1982).

[40] T. Uehlinger, G. Jotzu, M. Messer, D. Greif, W. Hofstetter, U. Bissbort, and T. Esslinger, Phys. Rev. Lett. **111**, 185307 (2013).

[41] P.-I. Schneider, S. Grishkevich, and A. Saenz, Phys. Rev. A **80**, 013404 (2009).

[42] Y. Chen, D.-W. Xiao, R. Zhang, and P. Zhang, Phys. Rev. A **101**, 053624 (2020).